LETTER • OPEN ACCESS

Ecological redline policy may significantly alter urban expansion and affect surface runoff in the Beijing-Tianjin-Hebei megaregion of China

To cite this article: Xinhui Ju *et al* 2020 *Environ. Res. Lett.* **15** 1040b1

View the article online for updates and enhancements.

Environmental Research Letters

LETTER

Ecological redline policy may significantly alter urban expansion and affect surface runoff in the Beijing-Tianjin-Hebei megaregion of China

Xinhui Ju[1], Weifeng Li[2] , Liang He[3], Junran Li[4], Lijian Han[2] and Jingqiao Mao[1]

[1] College of Water Conservancy and Hydropower Engineering, Hohai University, Nanjing 210098, People's Republic of China
[2] State Key Lab of Urban and Regional Ecology, Research Center for Eco-Environmental Sciences, Chinese Academy of Sciences, Beijing 100085, People's Republic of China
[3] Urumqi Natural Resources Comprehensive Survey Center of China Geological Survey, Urumchi 830057, People's Republic of China
[4] Department of Geosciences, The University of Tulsa, Tulsa, OK 74104, United States of America

E-mail: Li.wf@rcees.ac.cn

Abstract

Urban expansion leads to surface changes that disrupt hydrological processes and increases flooding risks in cities. This increase may be severe in urban megaregions where clusters of cites have agglomerated. The China Ecological Redline Policy (ERP) is a national policy that protects priority areas with high-value ecosystem services. However, it is not clear how the ERP alters megaregion expansion and what this means for surface runoff across entire regions. By integrating specified models, we developed future urban expansion scenarios for 2030 with and without the ERP in the Chinese Beijing-Tianjin-Hebei (BTH) megaregion. The annual surface runoff volume under the ERP scenario decreased by 78 million m^3 compared to the non-ERP involved scenario, but the ERP effectiveness at surface runoff regulation was different between the ecological redline areas (ERAs) and the non-ERAs. This suggested that multi-solutions should be incorporated into megaregions, such as regional ERPs and local, nature-based solutions, which could efficiently reduce the risk of urban flooding across whole regions.

1. Introduction

The development-environment conflict has become a major challenge across the globe, particularly in areas where rapid urbanization has increased the tension between urbanization, environmental protection, and economic growth (Bai *et al* 2012, Du *et al* 2018, Wing *et al* 2018). During the urban growth process, large areas of land are converted to impervious surfaces, which are known to affect surface runoff, and subsequent flood control and management in many urban areas (Trinh and Chui 2013, Hoekstra *et al* 2018, Zhang and Chui 2019). Increased runoff coefficients and shorter concentration times lead to increased flood risk (Nirupama and Simonovic 2007, Kjeldsen 2010, Guneralp *et al* 2015). Many cities have suffered urban flooding. For example, an urban flooding event that occurred in Beijing in 2012 caused 70 deaths and economic losses of 16 billion RMB (Wang *et al* 2020). Furthermore, city agglomeration is an important economic development strategy

in China. The government has promoted the emergence of large-scale urban agglomeration development modes. Many cities have now agglomerated and closely interact with each other. This has resulted in significant changes to land use patterns and surface runoff across a whole region rather than a single city (Day *et al* 2014, Sahana *et al* 2018). Therefore, it is very important to assess how the expansion of urban agglomeration affects surface runoff, and to explore possible measures and coordinated development in cities that could potentially improve flood mitigation.

Despite a growing need to find policy solutions that minimize the negative impacts of urban expansion on surface runoff, most practical solutions remain limited to local scales. At a local scale, the main actions have focused on urban storm water management, such as the introduction of low-impact development plans in the United States, the sustainable urban drainage system in the United Kingdom, and the sponge city proposed by China (Hamel *et al* 2013, Mcgrane 2015, Satyavati and Shirishkumar

2018). These efforts are effective solutions for regulating urban surface runoff that utilize the ecological functions (e.g. infiltration, storage, and interception) of specific land uses/covers. These are also known as nature-based measures and include green roofs, storm water parks, and permeable pavements, etc (Elliott and Trowsdale 2007, Imran *et al* 2013, Zolch *et al* 2017, Akther *et al* 2018, Du *et al* 2020). However, few studies have focused on mitigation solutions at larger scales, such as urban megaregions. This is due to the gathered development patterns of urban megaregions. These development patterns have led to more complicated land use/cover dynamics and consequent surface runoff than the ones found in individual cities. Some studies have shown that optimizing the spatial layout of megaregion expansion should reduce the risk of urban flooding (Wiering *et al* 2017).

The Ecological Redline Policy (ERP) was produced by the Chinese national government and its aim was to resolve the conflicts between regional conservation and development (Jia *et al* 2018). This policy has established priority conservation zones through the use of ecological redline areas (ERAs) at a regional scale, and these redline areas are based on ecosystem services assessments (Bai *et al* 2018). Ecosystem services are potentially important to human well-being, and are deemed an effective approach for identifying ERAs (Zhang *et al* 2020). Currently, the ERP is being promoted at the national scale (Jia *et al* 2018), and several provinces or cities are currently delimitating their ecological redline areas (Bai *et al* 2016). Some studies have assessed the effects of the ERP on urban expansion (Jia *et al* 2018, Bai *et al* 2018). For example, Bai *et al* (2018) found that the ERP in Shanghai led to a decrease in constructed area and an increase in forest compared to the baseline scenario. However, there has been no attempt to determine the most efficient ways of integrating the ERP into megaregion expansion and investigate the subsequent effects on surface runoff.

In this study, we examined the impact of the ERP on urban expansion and its potential effect on surface runoff across the Beijing-Tianjin-Hebei (BTH) megaregion in China. This large urban region is one of the most important megaregions in the eastern part of north China and is facing a serious development-environment conflict. The aims were to investigate (1) ways of integrating the ERP into megaregion expansion; (2) what effects the ERP would have on megaregion expansion; and (3) how the alterations to megaregion expansion by the ERP would further affect surface runoff in the megaregion. First, we simulated the future land use/cover patterns of the BTH megaregion under different scenarios. These were the regular trend scenario (RT), which did not consider the impact of the ERP, and the ecological protection scenario trend (EPT), which did include the ERP. Second, we simulated the annual surface runoff under the two different scenarios and analyzed

the impacts of different megaregion expansion scenarios on the surface runoff process at regional to subregional scales. Finally, we briefly discuss the policy and scientific implications of the results.

2. Methods

2.1. Land use/cover (LULC) scenarios
We created three LULC scenarios in order to analyze the differences due to LULC change with and without the ERP and the further effects on surface runoff in the BTH region. These scenarios were

Baseline 1 (BL) is a baseline scenario, which is the actual LULC map in 2015.

Scenario 1 (S1) is the regular trend (RT) scenario for 2030 without considering the impact of the ERP on LULC allocation.

Scenario 2 (S2) is an ecological protection trend (EPT) scenario for 2030, which considers the effect of the ERP.

2.2. Land use/cover classification
We used the Landsat-TM images from June–October, 2015 to generate the baseline land use/cover map (BL), with a spatial resolution of 30 m × 30 m. There are six land use/cover types in the BTH region, which are wetland, barren land, forest land, impervious land, grassland, and cultivated land. A backdating approach and an object-based method were integrated to identify the land use/cover types in 2015. We used the land use/cover classification of 2010 as the basic reference map to extract the changes in the land use/cover between 2010 and 2015, and then the change area was further classified. We used the stratified random sampling scheme to select locations within the cities and compared the image classifications to reference land use data created from the visual interpretation of high spatial resolution SPOT images (2.5 m) in eCognition Developer (www.ecognition.com/). The overall accuracy, Kappa statistic, and average producer and user accuracies exceeded 93%, 0.8, 80%, and 94%, respectively.

2.3. Evaluation of ecosystem services
A national ecosystem services assessment has been implemented in China (Ouyang *et al* 2016) and the assessment methods used in a previous study were applied to the BTH megaregion (Liu *et al* 2018). Based on the importance of ecosystem services to this megaregion and the availability of spatial data, we selected six ecosystem services and then used the national ecosystem services assessment methods to map ecological redline areas in the BTH region for 2015. The six services were soil retention, water retention, carbon sequestration, sand storm prevention, flood mitigation, and habitat provision for biodiversity. The data sources and data reliabilities are shown as table 1.

Table 1. Principal data sources.

Data	Resolution	Source
Ecosystem types	90 m, Landsat TM	the Institute of Remote Sensing Applications of the Chinese Academy of Sciences
Temperature	0.5 degree	China National Meteorological Information Center
DEM	90 m	the Shuttle Radar Topography Mission (SRTM)
Precipitation	1:6 000 000	China National Meteorological Information Center
Soil map and attribute data	1:1 000 000	China Soil Science Database
Evapotranspiration	90 m	the Institute of Geographic Sciences and Natural Resources Research, Chinese Academy of Science
Vegetation cover	250 m	Chinese Academy of Sciences
Aboveground biomass	250 m	Institute of Remote sensing and Digital Earth, Chinese Academy of Science
Average annual rainfall erosivity	-	Beijing Normal University

(1) Soil retention: this refers to soil reserved by ecosystems. The universal soil loss equation (USLE) was used to calculate soil retention, and was calculated by the InVEST model. The USLE can be expressed as follows (Yang *et al* 2016):

$$SC = R \times K \times LS \times (1 - C)$$

where *SC* represents the soil retention capacity (t/ha), *R* is the rainfall erosivity factor, *K* is the soil erodibility factor, *LS* is the topographic factor, and *C* is the vegetation cover factor.

Among them, *R* was calculated by the daily rainfall erosivity model and the input data was the daily precipitation data, which was acquired from the China National Meteorological Information Center; *K* was closely related to soil characteristics and was estimated using the erosion/productivity impact calculator (EPIC); the soil data was obtained from the China Soil Science Database; *LS* reflected the impact of slope length and steepness on soil retention and was calculated based on an empirical formula (Wei *et al* 2002); and *C* was obtained from relevant foreign and domestic literature (Wei *et al* 2002, Rao *et al* 2014).

(2) Water retention: This refers to water retained in ecosystems. Water retention was estimated using the water balance equation (Gong *et al* 2017):

$$TQ = (P - R - ET) \times A$$

where *TQ* is total water retention (m^3); *P* is precipitation (mm); *R* is storm runoff (mm); *ET* is evapotranspiration (mm); and *A* is the area of a specific ecosystem (m^2).

Major data inputs for the water retention calculation include rainfall data, runoff data, and evapotranspiration data for 2015. The evapotranspiration data were obtained from the Institute of Geographic Sciences and Natural Resources Research, Chinese Academy of Science. The storm runoff was calculated by multiplying precipitation by the runoff coefficient, which was estimated from previous studies (Gong *et al* 2017). All the input data were standardized and we used the spatial analyst tool in ArcGIS to calculate the total water retention.

(3) Carbon storage: this refers to the carbon in terrestrial ecosystems. After referring to the national ecosystem services assessment (Ouyang *et al* 2016), we calculated the biomass carbon storage of three ecosystem types in the BTH region. These were forest, grassland, and wetland ecosystems. The calculation formula is as follows (Lewis *et al* 2009):

$$BCS = B_i \times CC_i \times AR_i \times 10^{-6}$$

where *BCS* is the biomass carbon storage; B_i is the biomass density of ecosystem *i* (t/km^2), which was obtained from the Institute of Remote Sensing and Digital Earth, Chinese Academy of Science; CC_i is the carbon content in the ecosystem biomass, which is 0.5 for forest and wetland, and 0.45 for grassland (Fang *et al* 2010); and AR_i is the area of each grid cell.

(4) Sand storm prevention: This refers to sand reserved by ecosystems. We used the revised wind erosion equation (RWEQ) to estimate the sand storm prevention service, which was a function of the weather factor (*WF*), soil erodibility factor (*EF*), soil crust factor (*SCF*), surface roughness (*K'*), and vegetation cover parameter (*C*) (Borrelli *et al* 2017). The sand storm prevention volume was equal to the difference between the soil loss (S_L) under the bare land condition and the vegetation cover condition The RWEQ model can be expressed as follows:

$$Q_{max} = 109.8 \left[WF \times EF \times SCF \times K' \times C \right]$$
$$S = 150.71 \left(WF \times EF \times SCF \times K' \times C \right)^{-0.3711}$$
$$S_L = \frac{2 \times z}{S^2} Q_{max} \times e^{-(z/s)^2}$$

where Q_{max} is the maximum transport capacity (kg/m); S is the critical field length (m); Z is the distance from the upwind edge of the field (m); and S_L is the soil loss (kg/m²).

Among them, WF was calculated by dividing the total wind value for each period by 500 and multiplying by the number of days in the period (Ouyang *et al* 2016); the weather data were obtained from the China National Meteorological Information Center; EF reflected the relationship between wind erosion and soil physical and chemical properties; and SCF reflected the resistance of soil aggregates and crusts to windblown sand and was calculated using the SCF equation (Borrelli *et al* 2017). C has a significant effect on sand storm prevention and the vegetation cover data was acquired from the Chinese Academy of Sciences. The fraction of the ground surface covered with non-erodible plant material, and the silhouettes from standing plant residues and growing crop canopies were used in the RWEQ model to estimate the effect of vegetation cover (C) on sand storm prevention (Bilbro and Fryear 1994). The original RWEQ model was for the field scale, whereas our study was at a regional scale. Therefore, we used the roughness caused by the topography to replace the soil ridge roughness (K'), and was calculated using the Smith-Carson equation (Ouyang *et al* 2016).

(5) Flood mitigation: this refers to the flood mitigating volume of wetlands (e.g. lakes, reservoirs, and swamps). The national ecosystem services assessment (Ouyang *et al* 2016) was used to evaluate the flood mitigation capacity of various wetland types in the BTH megaregion. The area of wetlands was derived from the LULC data, and the storage capacity of wetlands was obtained from the Records for Chinese Lakes and The China Water Statistical Yearbook.

For lakes, available storage capacity was used as an indicator to measure flood mitigation capacity, which was a function of lake area (Ouyang *et al* 2016). The calculation formula is as follows:

$$Ln(C_l) = 1.128Ln(A) + 4.924$$

where C_l is the available storage capacity (10^4 m³) and A is the lake area (km²). The coefficient was obtained from Ouyang *et al* (2016).

For reservoirs, the flood control storage capacity (C_r) was used as the flood mitigating indicator (10^4 m³), which was calculated based on its total storage capacity ((10^4 m³)), and the coefficient was obtained from Ouyang *et al* (2016):

$$C_r = C_t \times 0.35$$

For swamps, the surface stagnation of water (C_s) was used as the flood mitigation indicator (10^4 m³). C_s was calculated by multiplying the swamp area (A (km²)) by the average maximum depth in a flood period (D (cm)), and 1 m was used as the depth

(Zhao *et al* 2003):

$$C_s = A \times D$$

(6) Provision of habitat for biodiversity: this refers to the total habitat area covered by indicator species. China performed a national biodiversity assessment in 2010 (Ouyang *et al* 2016). Due to the lack of species category and suitable habitat data, we adopted the corresponding evaluation results for the BTH region, which were based on the national assessment result (Ouyang *et al* 2016).

The national biodiversity assessment process was as follows: firstly, a total of 2820 species were selected as indicators to estimate biodiversity, including endemic, endangered, and nationally protected species. Then different protection targets (60%, 40%, or 30%) were assigned to species with different levels of rarity so that site selections could be carried out. Secondly, a habitat mapping process was developed using a simplified conceptual model (Xu *et al* 2009), and MARXAN (Klein *et al* 2010), a site selection software program, used an irreplaceability index to measure the biodiversity conservation value for each analytical unit. In our study, we used the 'high' and 'very high' areas of the national biodiversity assessment to delineate ecological redlines. The simplified conceptual model is as follows:

$$pH_i = C_i IH$$

where pH_i indicates whether polygon i is a potential habitat or not; C_i is the historical distributions of the indicator species in county i; I is the overlap of suitable elevation, slope, and aspect for the species; and H is suitable habitat for the species (Xu *et al* 2009).

2.4. Delineation of the ecological protection redline areas

We created an integrated index based on the six ecosystem services estimated above. This index, together with the information about ecosystem services and the relative abilities of different areas to supply them were used to map the ERAs.

The delineation of ERAs was undertaken using ArcGIS and the processes were as follows (Ouyang *et al* 2016): (1) we calculated the supply of each ecosystem service in a grid cell; (2) to quantify the relative importance of each grid cell for a single service, all grid cells were sorted by the supply of a specific ecosystem service in descending order, calculated the cumulative proportion of the specific ecosystem service across all grid cells, and then classified each grid into one of four levels of importance (very high, high, medium and normal). For example, we assigned 'very high' to the grids with cumulative proportion between 0% and 50%, 'high' to the grids with cumulative proportion between 50% and 75%, 'medium' to the grids with cumulative proportion between 75% and 90%, and 'normal' to the grids

with cumulative proportion between 90% and 100%; (3) By overlay analysis, the relative importance of each service was synthesized into a composite index of ecosystem service importance using the maximum values method. The composite index value equaled the highest importance value of any ecosystem service in each grid cell. Finally (4), the 'very high' and 'high' grid cells were defined as the ERAs.

2.5. Land use/cover scenarios

We used the CLUE-S model to simulate the different land use scenarios for 2030 (S1 (RT) and S2 (ERT)) based on the ERAs. The CLUE-S model is a spatially explicit model that can integrate the analysis of land use/cover change with the driving forces. The model mainly had two main parts, a non-spatial demand module and a spatially explicit allocation module (Verburg *et al* 1999, 2002). For the non-spatial module, the areal demands for different land use types on a yearly basis of the study area need to specify. Then, for the spatially explicit allocation module, the areal demands for different land use types will be allocated at specific location according to driving forces. The main advantages of this model were that it could simulate different scenarios and different land use/cover types at the same time by integrating spatial and non-spatial driving factors (Liu *et al* 2017a).

To simulate the LULC allocations in the BTH megaregion under the two different scenarios for 2030, in the RT scenario, we determined the yearly areal demands of different land use types based on the annual average LULC change from 2000 to 2015 by using the linear trend extrapolation (Liu *et al* 2018). In the EPT scenario, we determined the yearly areal demands of impervious land as similar to that in the RT scenario, while the areal demand of the wetlands, the forest, cultivated land a was according to the goals of the Wetland Conservation Plan (2015–2030) of Hebei, and the Master Plan (2006–2020) of Beijing, Tianjin and Hebei. Then the CLUE-S model allocated the areal land use demands for the time interval of one year. In the RT scenario, there was no spatial restrictions, and in the EPT scenario, the ecosystem redline areas were set as a spatial restriction.

The logistic regression model was used to identify the potential factors driving the spatial allocation of land use/cover (Islam *et al* 2018). We selected 14 driving forces based on previous research (Liu *et al* 2017b). These 14 driving forces were divided into three classes, which were the geographical, social, and economic factors (table 3). To simplify the analysis, all the variables were transformed into the raster format (Verburg *et al* 2002). In addition, the goodness of fit of the logistic regression model was evaluated using the curve of receiver operating characteristic (ROC) method, which can evaluate the predicted probabilities by comparing them with the observed values over the whole domain (Phung *et al* 2019). The area below

Table 2. CN values for the different land use/cover types in the Haihe basin.

Land use types	Hydrological soil group			
	A	B	C	D
Wetland	98	98	98	98
Barren land	77	86	91	94
Forest land	48	68	79	85
Impervious land	89	92	94	96
Grassland	52	74	81	86
Cultivated land	64	75	82	86

the ROC curve represents the ROC value, whose prediction accuracy improves as the value gets closer to 1 (Lamichhane and Shakya 2019).

Finally, we used the CLUE-S model to generate future land use scenarios. The Kappa coefficient was used to assess the effectiveness of the CLUE-S model. It evaluates simulated probabilities by comparing them with ideal probabilities. In this study, the LULC simulation result for 2015 was compared with the interpreted LULC map to calibrate the land use type specific conversion and assess the accuracy of the CLUE-S model.

2.6. Simulation of average annual surface runoff

We estimated the average annual surface runoff under different land use scenarios using the long-term hydrological impact assessment (L-THIA) model, which was developed by Purdue University in the United States.

The L-THIA model is a distributed hydrological model, and can be used to simulate surface runoff on a large spatial-temporal scale (Lim *et al* 2006). The L-THIA model is based on the SCS-CN (Soil Conservation Service-Curve Number) method (Shadeed and Almasri 2010, Li *et al* 2018), which simulates the runoff volume for each grid cell from the *CN* value and daily rainfall. The *CN* value is a dimensionless parameter that comprehensively reflects land use type, soil group, and antecedent moisture conditions (Bhaduri *et al* 2000).

The calculation formula for the L-THIA model is as follows:

$$\begin{cases} Q = \frac{(P - I_a)^2}{(P - I_a) + S}, I_a < P \\ Q = 0, I_a \geq P \end{cases}$$

$$I_a = 0.2S$$

$$S = \frac{1000}{CN} - 10$$

where, Q is runoff (mm); P is rainfall (mm); I_a is initial abstraction (mm); and S is potential maximum retention after runoff begins.

Table 3. Factors driving land use pattern in the Beijing-Tianjin-Hebei urban cluster.

Types	Driving factors	EXP(B)					
		Wetland	Barren land	Forest land	Impervious land	Grassland	Cultivated land
Geographical factors	Elevation/m	-	0.999	1.001	0.999	0.999	0.999
	Slope/°	0.750	0.886	1.296	0.874	0.973	0.748
	Distance to river/km	1.006	1.003	-	-	1.004	0.997
	Distance to coastline/km	0.992	1.003	0.995	1.002	1.008	1.003
	Distance to railway/km	1.009	0.994	0.982	0.998	-	1.011
	Distance to national highway/km	1.018	1.031	1.007	-	1.018	0.983
	Distance to highway/km	0.997	1.016	1.01	0.994	0.998	0.995
Social factors	Distance to downtown/km	1.015	-	1.005	1.002	0.998	0.997
	Distance to Beijing and Tianjin/km	0.996	1.009	1.002	-	0.997	0.999
	Proportion of urban population/%	1.045	1.214	0.937	-	1.147	1.01
	Proportion of secondary industry/%	-	0.739	1.115	-	0.73	0.956
Economic factors	Proportion of tertiary industry%	0.97	0.7	1.181	0.987	0.722	0.934
	Light intensity index (I)	-	4.675	0.243	18.812	1.446	0.267
	Light area index (S)	-	-	0.521	3.586	1.454	0.619
	Constant	−3.897	10.239	−9.412	−3.500	16.231	4.903
	ROC	0.876	0.800	0.907	0.858	0.783	0.872

Notes: EXP(B) refers to e^{B}, where B is the beta coefficient for each variable in the logistic regression model. Constant refers to the constant term for each variable in the logistic regression result.

The data required for the model included land use data, soil data, hydrological data, and meteorological data. The soil data for the BTH megaregion were obtained from the China Soil Database and classified into four categories (A, B, C, and D) according to the classification standard of the United States Department of Agriculture, as required for L-THIA model. Soil permeability decreased from A to D. The daily runoff data from 1950 to 2015 were used to operate the L-THIA model and were acquired from The China National Meteorological Information Center. The L-THIA model was validated using observed runoff data from Luanxian reservoir, Wangkuai reservoir, and Xidayang reservoir, and the relative error was ± 10%, which indicated that the model could accurately simulate the surface runoff in the BTH region (Ju *et al* 2020) (figure 1). The CN values for the BTH region were obtained from Ju *et al* (2020) and are shown in table 2.

The surface runoff volume is closely related to the size of accumulated surface area. Therefore, we used the normalized average annual runoff depth (*NAARD*) to characterize the surface runoff generation ability by eliminating the impact of city size on surface runoff. The calculation formula is as follows (Chen *et al* 2017):

$$NAARD_{city} = \frac{RV_{city}}{A_{city}} \times 1000$$

where $NAARD_{city}$ is the normalized average annual runoff depth for a city (mm); RV_{city} is the average annual runoff volume for a city (m^3); and A_{city} is the administrative area of a city (m^2).

3. Results

3.1. The ecological redline areas in the BTH region
In general, the ERAs covered about 106 173.36 km^2 in total and accounted for 49.53% of the BTH region (figure 2). The spatial distribution of the ERAs in the BTH region was uneven, and the northern and western mountains, the eastern Bohai Bay coastline, and inland lakes were the primary ecological reserves.

The ecosystem services within the ERAs also had different spatial distributions (figure 2). Within the ERAs, the soil retention conservation areas were concentrated in the Yanshan and Taihangshan mountains in the northern and western parts of the BTH region. They covered 103 245.10 km^2. Water retention zones within the ecological redline areas covered 72 277.81 km^2. They were mainly distributed along the eastern coastlines, in inland lakes, and the boundary between mountains and plains. Carbon sequestration areas within the ERAs were mainly distributed in the Yanshan Mountains of the northern BTH region, and their area covered 69 405.00 km^2 in total. Sand storm prevention and conservation areas covered 59 637.20 km^2, and only occurred in the northwestern forest of the BTH region. The

flood mitigation area distribution was similar to water retention and the area within the redline area covered 81 510.50 km^2. The biodiversity areas covered 31 845.79 km^2, and mainly occurred in the northern, central, and southern parts of the BTH region.

3.2. Urban expansion of the BTH megaregion under the different scenarios
The logistic regression results are shown in table 3. The ROC value for each LULC type was greater than 0.7, which indicated that the regression model was suitable. Comparing the LULC simulation result with the interpreted LULC map for 2015 allowed us to obtain a Kappa coefficient of 0.79, which showed that the CLUE-S model performed satisfactorily.

The total BTH megaregion expansion patterns for 2030 under the different scenarios were similar, but the change ranges for the different LULC types varied (figure 3, table 4). For example, the increases in impervious land across the BTH megaregion under the two 2030 scenarios were similar when compared to the baseline scenario in 2015, but their spatial occurrence was distinct. The impervious land in the BTH megaregion increased by 26.34% under the RT scenario relative to 2015 and increased by 25.02% under the EPT scenario. A comparison of the RT and EPT scenarios showed that there was an obvious difference in urban expansion inside and outside the ERAs. Inside the ERAs, the increase in impervious land was 1890 km^2 under the RT scenario for 2030 relative to 2015, but there was no increase under the EPT scenario. Outside the ERAs, the increase in impervious land was 411.04 km^2 under the RT scenario for 2030 relative to 2015, whereas the increase was 5707.08 km^2 under the EPT scenario. The increase in impervious land outside the ERAs under the EPT scenario for 2030 was about 1589.04 km^2 more than under the RT scenario relative to the baseline in 2015. For example, the increase in impervious land across Baoding and Handan under the EPT scenario was 94.32 and 104.04 km^2 more than under the RT scenario, respectively.

In addition, the cultivated land decreased under both 2030 scenarios, but the cultivated land under the EPT scenario decreased slightly less than that under the RT scenario. In contrast, under the EPT scenario, there was substantial increase in wetland relative to the RT scenario. For example, the total wetland area for 2030 under the EPT scenario increased by 9.20% compared to 2015, but decreased by 8.36% under the RT scenario. The forest area under the EPT scenario increased 221.04 km^2 more than under the RT scenario. The most obvious difference in land use change between the RT and EPT scenarios occurred in the northern part of the BTH megaregion, especially in Beijing, Chengde, and Zhangjiakou. In contrast, the land use changes in the other regions within the BTH megaregion were similar under the two future scenarios.

Table 4. Land use type areas in the Beijing–Tianjin–Hebei urban agglomeration.

| Land use types	Baseline scenario		Trend prediction scenario			Ecological protection scenario		
	Area /km^2	Percentage /%	Area /km^2	Percentage /%	change rate/%	Area/km^2	Percentage /%	change rate/%
Wetland	5688.72	2.65	5213.16	2.43	−8.36	6212.16	2.90	9.20
Barren land	663.12	0.31	641.88	0.30	−3.20	424.44	0.20	−35.99
Forest land	71 111.52	33.18	71 278.92	33.25	0.24	71 499.96	33.36	0.55
Impervious land	22 806.72	10.64	28 814.76	13.44	26.34	28 513.8	13.30	25.02
Grassland	19 983.96	9.32	21 373.56	9.97	6.95	20 372.4	9.50	1.94
Cultivated land	94 092.12	43.90	87 023.88	40.60	−7.51	87 323.4	40.74	−7.19
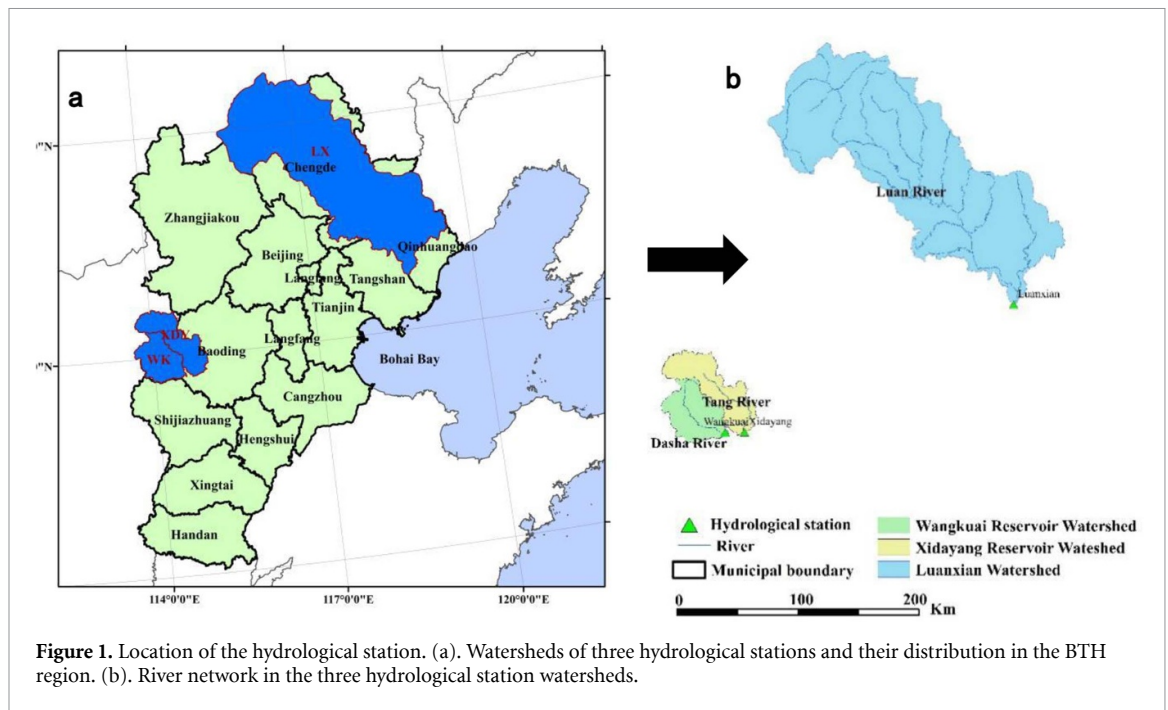
Figure 1. Location of the hydrological station. (a). Watersheds of three hydrological stations and their distribution in the BTH region. (b). River network in the three hydrological station watersheds.

At the sub-region level, the impervious land in most cities across the BTH megaregion had expanded by 2030 relative to 2015 under both 2030 scenarios, but there were certain differences between the scenarios (table 5). Generally, there were two major differences between the two 2030 scenarios. In one case, urban expansion under the EPT scenario was less than under the RT scenario. There were three cities following this type of expansion, which were Beijing, Tianjin, and Chengde. The largest decrease in impervious land had occurred in the mega-city of Beijing by 2030 under the EPT scenario compared to the RT scenario, and the reduced area was 697.32 km^2. There were ten cities where urban expansion under the EPT scenario for 2030 was faster than under the RT scenario. Among these cities, the largest increase in impervious land by 2030 under the EPT scenario occurred in Zhangjiakou, at 156.24 km^2.

3.3. Impacts of BTH megaregion expansion on surface runoff under the different scenarios

Generally, on regional scale, the total average annual surface runoff for the entire BTH megaregion by 2030 under both the EPT and RT scenarios increased relative to that in 2015 (table 6). The total surface runoff for 2030 under the RT scenario increased by 5.87% (8.46 hundred million m^3) relative to 2015, and increased by 5.33% (7.68 hundred million m^3) under the EPT scenario. The megaregion expansion under the EPT scenario reduced potential surface runoff by 78 million m^3 across the entire BTH megaregion compared to the RT scenario. In addition, the contributions of the different land use/cover types to surface runoff across the BTH megaregion were different. What was noteworthy was that the surface runoff generated from impervious land made the largest

contribution to the total runoff among all land use/cover types in 2030, whereas it was farmland that contributed the most to total runoff in 2015. The contribution to surface runoff made by impervious land was 32.83% in 2015, and will be 38.56% and 38.68% in 2030 under the RT and EPT scenarios, respectively.

There was an obvious difference in the surface runoff change between inside and outside the ERAs from 2015 to 2030 under the RT and EPT scenarios (table 7). The total surface runoff for 2030 under the EPT scenario decreased by 4.45% (2.57 hundred million m^3) relative to the RT scenario inside the ERAs, whereas it increased by 1.88% (1.78 hundred million m^3) outside the ERAs. Furthermore, in the two future scenarios, forest land made the largest contribution to the surface runoff inside the ERAs because it accounted for 50% of the total surface runoff. Impervious land and cultivated land had the two highest surface runoff contribution rates outside the ERAs, and the total contribution made by the two land use types exceed 90% under both future scenarios.

At the city scale, the normalized average annual runoff depth (*NAARD*) for most cities increased under both the RT and EPT scenarios by 2030 relative to that in 2015, but there were also distinct among cities for the two scenarios (figure 4, table 8). Compared to the baseline scenario in 2015, Tianjin city showed the largest increase (17.71 mm) in *NAARD*, followed by Beijing (10.82 mm) under the RT scenario. In contrast, under the EPT scenario, Tianjin city also showed the largest increase in *NAARD* at 15.96 mm, but Beijing was ranked fourth (6.04 mm). Thus, the impacts of the ERP on the different cities in terms of city-level surface runoff were different to the RT scenario. There were three cities where the ERP could reduce the *NAARD* relative to the RT

Table 5. Impervious land areas under the three scenarios and the change rate compared to the baseline scenario in the different cities.

Cities	Baseline scenario Area/km²	Regular trend scenario			Ecological protection trend scenario		
		Area/km²	Increased area relative to 2015/km²	Increase in rate relative to 2015/%	Area/km²	Increased area relative to 2015/km²	Increase in rate relative to 2015/%
Beijing	2990.16	4632.12	1641.96	54.91	3934.80	944.64	31.59
Tianjin	2800.44	3925.44	1125.00	40.17	3791.52	991.08	35.39
Tangshan	2261.52	2802.24	540.72	23.91	2821.32	559.80	24.75
Qinhuangdao	682.92	929.16	246.24	36.06	936.00	253.08	37.06
Chengde	679.32	942.12	262.80	38.69	916.20	236.88	34.87
Zhangjiakou	1361.16	1459.08	97.92	7.19	1615.32	254.16	18.67
Baoding	2464.92	2762.64	297.72	12.08	2856.96	392.04	15.90
Shijiazhuang	1915.56	2275.92	360.36	18.81	2328.12	412.56	21.54
Langfang	1181.52	1683.72	502.20	42.50	1712.52	531.00	44.94
Cangzhou	1864.80	2150.28	285.48	15.31	2172.96	308.16	16.53
Hengshui	1273.32	1363.32	90.00	7.07	1377.72	104.40	8.20
Xingtai	1588.68	1704.24	115.56	7.27	1761.84	173.16	10.90
Handan	1742.40	2184.48	442.08	25.37	2288.52	546.12	31.34

Table 6. Annual surface runoff due to the various land use/cover types in the BTH megaregion under the different scenarios.

Scenarios	Baseline scenario		Regular trend scenario			Ecological protection trend scenario		
	Runoff /10^8 m^3	Percentage /%	Runoff /10^8 m^3	Percentage /%	Runoff change /10^8 m^3	Runoff /10^8 m^3	Percentage /%	Runoff change /10^8 m^3
Barren land	0.82	0.57%	0.80	0.52%	−0.02	0.48	0.32%	−0.34
Forest land	33.39	23.16%	33.33	21.84%	−0.06	33.50	22.06%	0.10
Impervious land	47.33	32.83%	58.85	38.56%	11.52	58.74	38.68%	11.42
Grassland	10.62	7.37%	11.27	7.39%	0.65	10.79	7.10%	0.16
Cultivated land	52.01	36.07%	48.38	31.69%	−3.63	48.34	31.84%	−3.66
Total	144.17	1.00	152.63	100.00%	8.46	151.85	100.00%	7.68

Note: the runoff changes under the RT and the EPT scenarios were calculated by comparing the results to the baseline scenario.
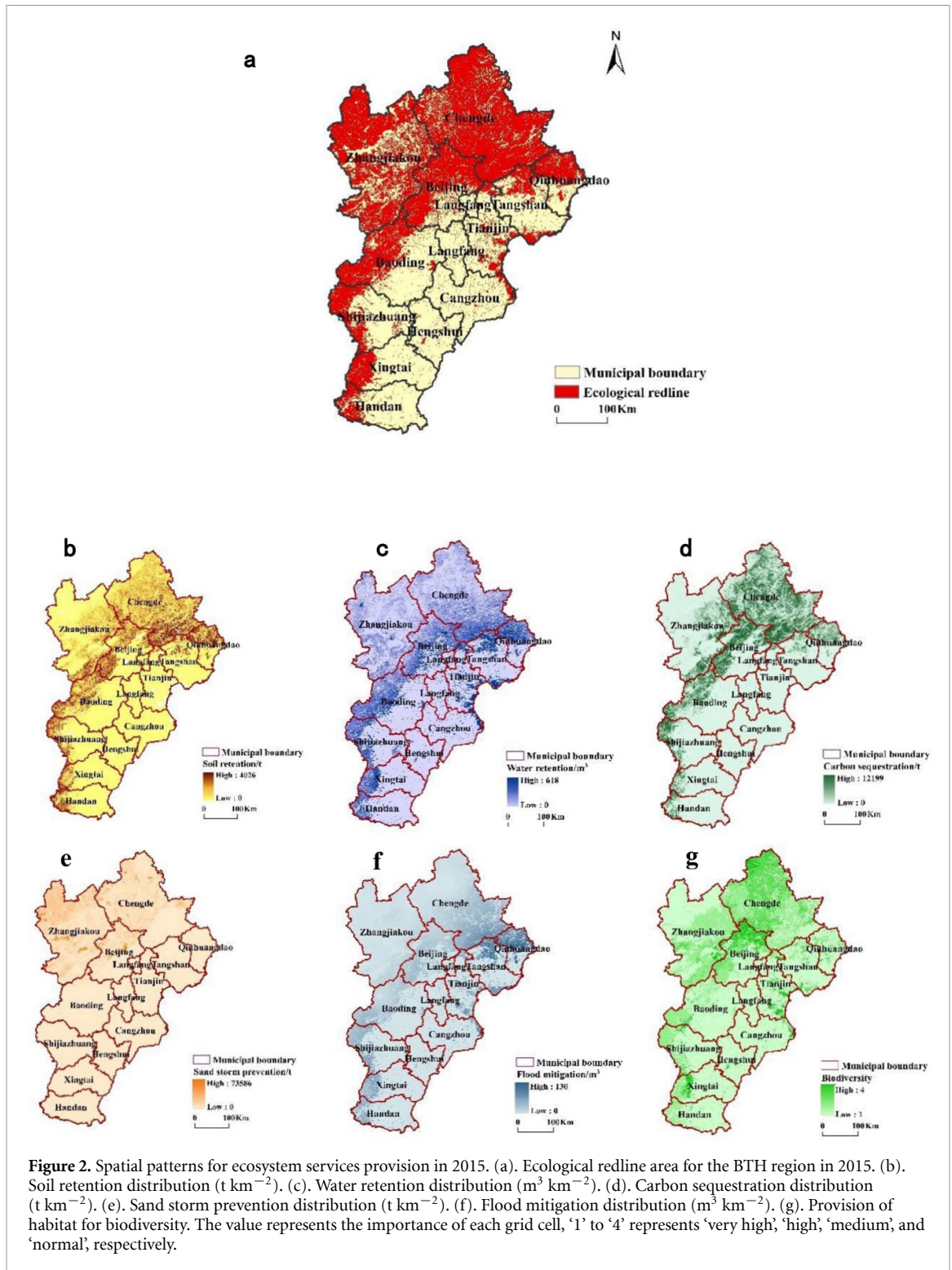
Figure 2. Spatial patterns for ecosystem services provision in 2015. (a). Ecological redline area for the BTH region in 2015. (b). Soil retention distribution (t km^{-2}). (c). Water retention distribution (m^3 km^{-2}). (d). Carbon sequestration distribution (t km^{-2}). (e). Sand storm prevention distribution (t km^{-2}). (f). Flood mitigation distribution (m^3 km^{-2}). (g). Provision of habitat for biodiversity. The value represents the importance of each grid cell, '1' to '4' represents 'very high', 'high', 'medium', and 'normal', respectively.

scenario. For example, the *NAARD* for Beijing by 2030 under the EPT scenario decreased by 4.79 mm (−5.52%) relative to that under the RT scenario. In contrast, the urban expansion under the EPT scenario might increase the *NAARD* of ten cities compared to the RT scenario. Among these cities, Handan showed the largest *NAARD* increase. The EPT results for Handan showed that there would be an additional 1.71 mm (1.75%) of *NAARD* relative to the RT scenario.

4. Discussion

Under the current development trends, megaregions in China will continue to expand, and this will inevitably intensify the conflicts between development and the environment (Fang *et al* 2018). This is a considerable challenge that decision makers must confront. Our results showed that under the RT scenario for 2030, surface runoff in the BTH would increase by 8.46 hundred million m^3 in total, compared to the
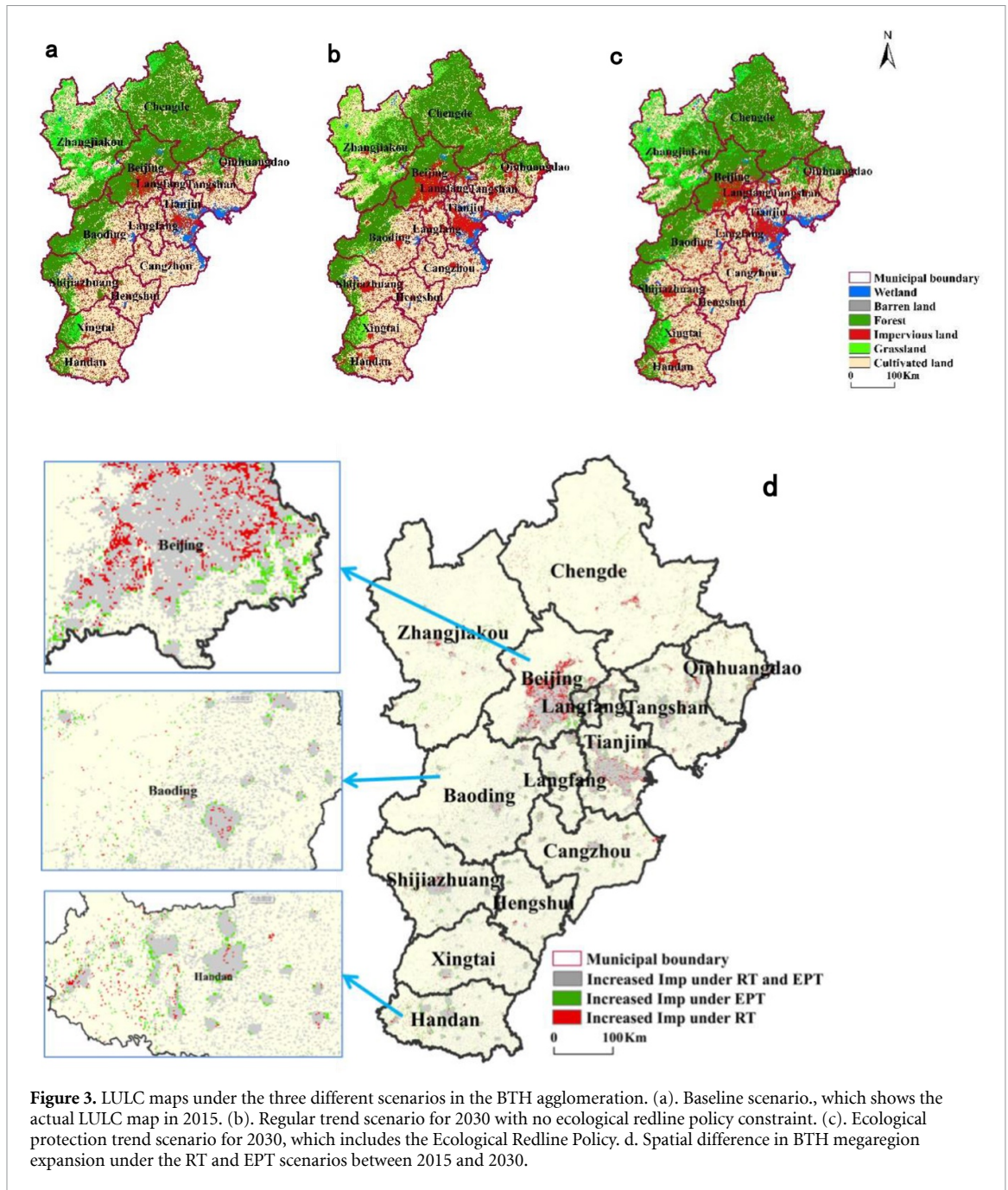
Figure 3. LULC maps under the three different scenarios in the BTH agglomeration. (a). Baseline scenario., which shows the actual LULC map in 2015. (b). Regular trend scenario for 2030 with no ecological redline policy constraint. (c). Ecological protection trend scenario for 2030, which includes the Ecological Redline Policy. d. Spatial difference in BTH megaregion expansion under the RT and EPT scenarios between 2015 and 2030.

Table 7. Average annual surface runoff rates inside and outside the ERAs under the two future scenarios in the BTH megaregion.

Scenarios	Regular trend scenario		Ecological protection scenario	
	Inside the ERAs /10^8 m^3	Outside the ERAs /10^8 m^3	Inside the ERAs /10^8 m^3	Outside the ERAs /10^8 m^3
Barren land	0.46	0.34	0.47	0.01
Forest land	29.78	3.56	29.87	3.63
Impervious land	9.68	49.17	6.27	52.47
Grassland	9.35	1.92	8.96	1.83
Cultivated land	8.51	39.87	9.65	38.70
Total	57.78	94.86	55.21	96.64

baseline in 2015, which is nearly 1/3 of total domestic water consumption in Beijing. This may reduce the already limited water resources and increase the flood risk that the BTH megaregion is currently facing (Li *et al* 2020). Therefore, researchers and policy makers

in China need to minimize the negative impact of megaregion expansion on surface runoff.

Our study attempted to explore whether the national ecological redline policy has an effect on surface runoff across a large urban megaregion in China,

Table 8. Normalized average annual runoff depths (*NAARD*) for the different cities.

| Cities	Baseline scenario	Trend prediction scenario		Ecological protection scenario	
	NAARD/mm	*NAARD*/mm	*NAARD* change/mm	*NAARD*/mm	*NAARD* change/mm
Beijing	75.95	86.77	10.82	81.99	6.04
Tianjin	85.90	103.61	17.71	101.86	15.96
Tangshan	61.13	66.30	5.17	66.78	5.64
Qinhuangdao	67.53	71.66	4.13	72.34	4.81
Chengde	35.50	35.99	0.49	36.17	0.66
Zhangjiakou	51.25	51.27	0.02	51.82	0.57
Baoding	115.35	118.42	3.06	118.98	3.62
Shijiazhuang	123.88	128.50	4.61	128.90	5.02
Langfang	57.92	67.98	10.07	68.50	10.58
Cangzhou	49.01	52.38	3.38	52.47	3.46
Hengshui	48.32	50.38	2.06	50.36	2.04
Xingtai	91.18	92.78	1.60	93.54	2.36
Handan	91.74	97.83	6.09	99.55	7.80
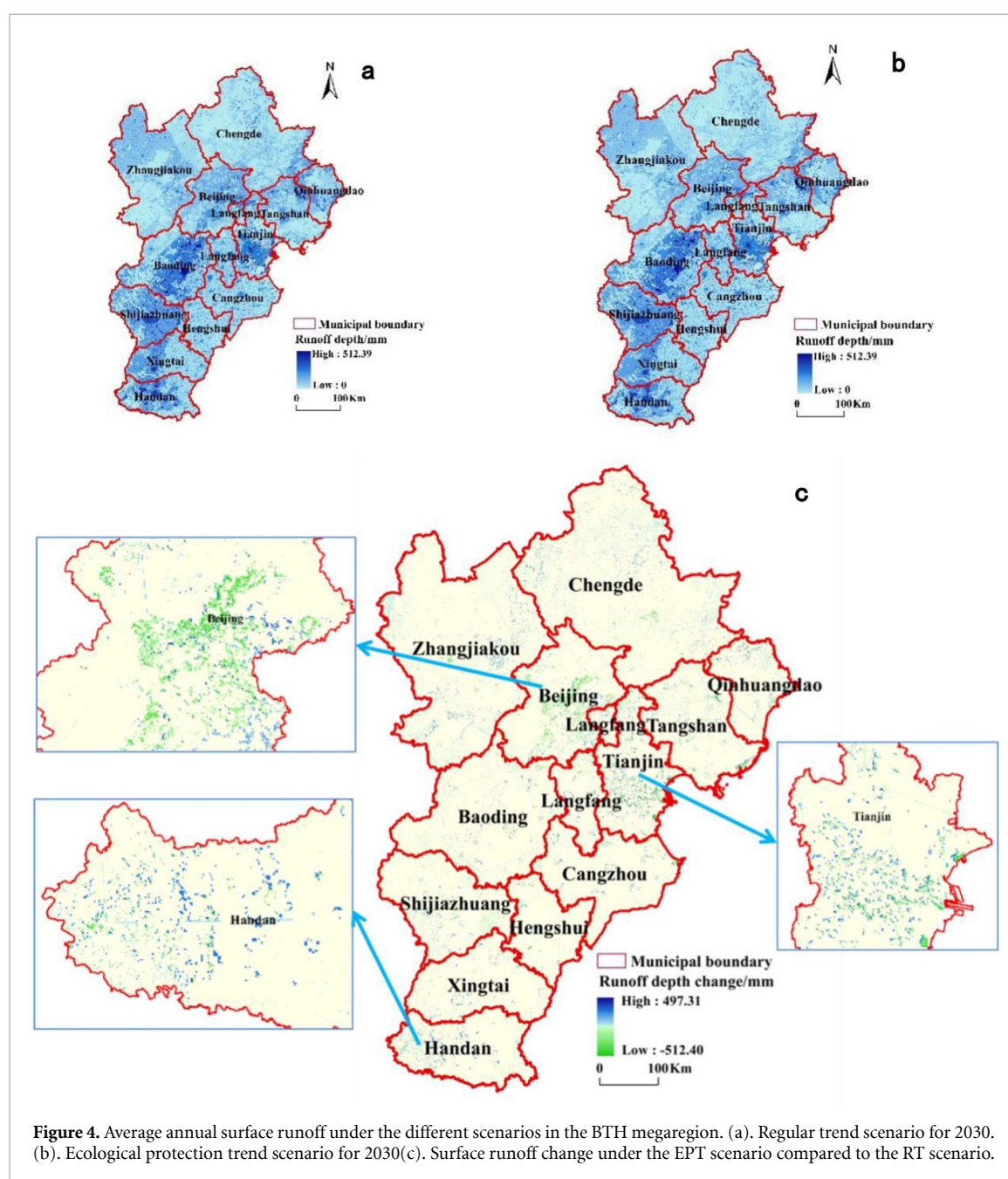
Figure 4. Average annual surface runoff under the different scenarios in the BTH megaregion. (a). Regular trend scenario for 2030. (b). Ecological protection trend scenario for 2030(c). Surface runoff change under the EPT scenario compared to the RT scenario.

and through scenario analysis, we found megaregion expansion under the EPT scenario can result in a lower surface runoff increase relative to the RT scenario. This finding revealed that altering urban expansion under the ERP scenario can protect the specific priority areas that have important ecological services, and reduce overall surface runoff generation by the megaregion. Although the surface runoff reduction (0.78 hundred million m^3) under the EPT scenario relative to RT scenario was limited, this study shows the potential value of the policy-making alternatives when attempting to promote the development of large-scale megaregions. Our findings also confirmed the results of previous studies that investigated these effects at individual city scales. For example, Bai *et al* (2012) reported that the inclusion of the ERP in urban land use planning in metropolitan Shanghai, China, increased terrestrial habitat protection by 174% and maintained flood mitigation.

Our results also showed the different runoff changes inside and outside the ERAs under the EPT and RT scenarios. They showed that the impacts of the ERP on different sub-regions of the BTH megaregion were distinct. Although the surface runoff generated inside the ERAs under the EPT scenario was much less than that under the RT scenario, the greater surface runoff generation outside the ERAs under the EPT scenario may offset some of the surface runoff reduction within the ERAs relative to the RT scenario. This is because the inclusion of the ERP into the megaregion expansion plans prohibited the growth of impervious land within the ERAs, and thus, promoted an increase in impervious land outside the areas in order to maintain the same expansion rate for the entire region under the EPT scenario as would occur under the RT scenario. This leads to more potential surface runoff generation outside the ERAs under the EPT scenario than under the RT scenario. Therefore, these results emphasize that the implementation of the ERP alone into the spatial land use planning for megaregion expansion may be insufficient to reduce the surface runoff in all sub-regions within the megaregion. In the case of the BTH megaregion, cities, such as Handan and Baoding, which are not included in the ecological redline areas, need to have more urban expansion to compensate for the urban growth constraints in ERAs. Therefore, sub-regional solutions need to be created for these cities in order to regulate urban surface runoff. There are already some effective city-level solutions that mitigate surface runoff, such as low-impact development measures (Wang *et al* 2020). Therefore, if joint regional-level ERP and sub-regional solutions are integrated into the spatial planning policies for megaregions, then surface runoff would be efficiently minimized in both regions and sub-regions.

Our study also had some limitations. For example, there is no standardized approach for identifying ERAs due to the diversity and complexities of ecosystem services. Furthermore, it was difficult to acquire high-quality data, and parameterize and interpret models etc. These limitations could lead to difficulties when attempting to identify potential ERAs. Therefore, there is a need to standardize procedures for these issues so that the identification of ERAs can become more effective. Additionally, the quality of the driving factors data used for the urban expansion simulation may have affected modeling accuracy. Furthermore, during model calibration (L-THIA model), the lack of available data might have affected the modeling reliability. We also did not consider the impacts of future climate change on surface runoff, which will play an important role in runoff generation. In further studies, alternative models and higher-quality data could be used to simulate urban expansion patterns and hydrological processes.

5. Conclusions

This study proposes a new way to examine the effectiveness of including the ERP in large-scale urban megaregions by analyzing how the ERP can alter urban expansion and effect the alteration on surface runoff. Through scenario analysis, the inclusion of the ERP into BTH megaregion expansion plans could reduce the annual surface runoff in the entire region while maintaining a similar growth rate for urban expansion envisaged under the RT scenario. We showed that the ERP effectively promoted urban expansion and regulated surface runoff in megaregions. These findings will significantly affect sustainable development, and urban flood control and management. However, the impacts of the ERP on surface runoff were distinct within and beyond the ERAs. The increase in surface runoff outside the ERAs may offset some of the surface runoff reduction when the EPT scenario is compared to the RT scenario. This implies that the ERP alone may not be able to mitigate surface runoff in all cities within megaregions. Integrating regional ERPs with beyond-ERA solutions can help minimize the effects of urban expansion on surface runoff at the sub-regional scale Our study has the potential to be scaled up to find modes of sustainable growth in urban megaregions throughout and beyond China.

Data availability statement

The data that support the findings of this study are available upon reasonable request from the authors.

ORCID iD

Weifeng Li ⓘ https://orcid.org/0000-0003-1212-4345

References

Akther M, He J, Chu A, Huang J and van Duin B 2018 A review of green roof applications for managing urban stormwater in different climatic zones *Sustainability* **10** 2864

Bai X, Chen J and Shi P 2012 Landscape urbanization and economic growth in China: positive feedbacks and sustainability dilemmas *Environ. Sci. Technol.* **46** 132–9

Bai Y, Jiang B, Wang M, Li H, Alatalo J M and Huang S 2016 New ecological redline policy (ERP) to secure ecosystem services in China *Land Use Policy* **55** 348–51

Bai Y, Wong C P, Jiang B, Hughes A C, Wang M and Wang Q 2018 Developing China's ecological redline policy using ecosystem services assessments for land use planning *Nat. Commun.* **9** 3034

Bhaduri B, Harbor J, Engel B and Grove M 2000 Assessing watershed-scale, long-term hydrologic impacts of land-use change using a GIS-NPS model *Environ. Manage.* **26** 643–58

Bilbro J D and Fryear D W 1994 Wind erosion losses as related to plant silhouette and soil cover *Agron. J.* **86** 550–3

Borrelli P, Lugato E, Montanarella L and Panagos P 2017 A new assessment of soil loss due to wind erosion in European agricultural soils using a quantitative spatiality distributed modelling approach *Land Degrad. Dev.* **28** 335–44

Chen J, Theller L, Gitau M W, Engel B A and Harbor J M 2017 Urbanization impacts on surface runoff of the contiguous United States *J. Environ. Manage.* **187** 470–81

Day J W, Moerschbaecher M, Pimentel D, Hall C and Yáñez-Arancibia A 2014 Sustainability and place: how emerging mega-trends of the 21st century will affect humans and nature at the landscape level *Ecol. Eng.* **65** 33–48

Du S *et al* 2020 Hard or soft flood adaptation? Advantages of a hybrid strategy for Shanghai *Glob. Environ. Change* **61** 102037

Du S, He C, Huang Q and Shi P 2018 How did the urban land in floodplains distribute and expand in China from 1992–2015? *Environ. Res. Lett.* **13** 034018

Elliott A H and Trowsdale S A 2007 A review of models for low impact urban stormwater drainage *Environ. Model. Softw.* **22** 394–405

Fang C, Bao C, Huang J and Li G 2018 Contribution, responsibility and mission of geography on China's urbanization development (in Chinese) *Sci. Geographica Sin.* **38** 321–31

Fang J, Yang Y, Ma W, Mohammat A and Shen H 2010 Ecosystem carbon stocks and their changes in China's grasslands *Sci. China Life Sci.* **53** 757–65

Gong S, Xiao Y, Zheng H, Xiao Y and Ouyang Z 2017 Spatial patterns of ecosystem water conservation in China and its impact factors analysis (In Chinese) *Acta Ecologica Sin.* **37** 2455–62

Guneralp B, Guneralp I and Liu Y 2015 Changing global patterns of urban exposure to flood and drought hazards *Glob. Environ. Change* **31**: 217–25

Hamel P, Daly E and Fletcher T D 2013 Source-control stormwater management for mitigating the impacts of urbanisation on baseflow: A review *J. Hydrol.* **485** 201–11

Hoekstra A Y, Buurman J and van Ginkel K C H 2018 Urban water security: A review *Environ. Res. Lett.* **13** 053002

Imran H M, Akib S and Karim M R 2013 Permeable pavement and stormwater management systems: A review *Environ. Technol.* **34** 2649–56

Islam K, Rahman M F and Jashimuddin M 2018 Modeling land use change using cellular automata and artificial neural network: the case of Chunati wildlife sanctuary, Bangladesh *Ecol. Indic.* **88** 439–53

Jia Z, Ma B, Zhang J and Zeng W 2018 Simulating spatial-temporal changes of land-use based on ecological redline restrictions and landscape driving factors: a case study in Beijing *Sustainability* **10** 1299

Jiang W, Chen Z, Lei X, Jia K and Wu Y 2015 Simulating urban land use change by incorporating an autologistic regression model into a CLUE-S model *J. Geog. Sci.* **25** 836–50

Ju X *et al* 2020 Effects of land use change on surface runoff in Beijing-Tianjin-Hebei urban agglomeration (In Chinese) *Acta Ecologica Sin.* **40** 1–11

Kjeldsen T R 2010 Modelling the impact of urbanization on flood frequency relations in the UK *Hydrol. Res.* **41** 391–405

Klein C J, Steinback C, Watts M, Scholz A J and Possingham H P 2010 Spatial marine zoning for fisheries and conservation *Frontiers Ecol. Environ.* **8** 349–53

Lamichhane S and Shakya N M 2019 Integrated assessment of climate change and land use change impacts on hydrology in the Kathmandu Valley watershed, Central Nepal *Water* **11** 2059

Lewis S L *et al* 2009 Increasing carbon storage in intact African tropical forests *Nature* **457** 1003–6

Li C, Liu M, Hu Y, Shi T, Qu X and Walter M T 2018 Effects of urbanization on direct runoff characteristics in urban functional zones *Sci. Total Environ.* **643** 301–11

Li W, Hai X, Han L, Mao J and Tian M 2020 Does urbanization intensify regional water scarcity? Evidence and implications from a megaregion of China *J. Clean. Prod.* **244** 118592

Lim K J, Engel B A, Muthukrishnan S and Harbor J 2006 Effects of initial abstraction and urbanization on estimated runoff using CN technology *Ecol. Indic.* **42** 629–43

Liu G, Jin Q, Li J, Li L, He C, Huang Y and Yao Y 2017a Policy factors impact analysis based on remote sensing data and the CLUE-S model in the Lijiang River Basin, China *Catena* **158** 286–97

Liu J, Li W, Zhou W, Han L and Qian Y 2018 Prediction of expansion pattern and impact on regional ecological security of Beijing-Tianjin-Hebei metropolitan region (In Chinese) *Acta Ecologica Sin.* **38** 1650–60

Liu J, Li W, Zhou W, Han L, Qian Y and Zheng X 2017b Simulation and prediction of changes in the landscape patterns of the Beijing-Tianjin-Hebei metropolitan region and their driving mechanisms (In Chinese) *Acta Ecologica Sin.* **37** 5324–33

McGrane S J 2015 Impacts of urbanization on hydrological and water quality dynamics, and urban water management: a review *Hydrological Sciences Journal* **61** 2295–311

Nirupama N and Simonovic S P 2007 Increase of flood risk due to urbanisation: a Canadian example *Nat. Hazard.* **40** 25–41

Ouyang Z *et al* 2016 Improvements in ecosystem services from investments in natural capital *Science* **352** 1455–9

Phung Q A, Thompson A L, Baffaut C, Costello C, Sadler E J, Svoma B M, Lupo A and Gautam S 2019 Climate and land use effects on hydrologic processes in a primarily rain-fed, agricultural watershed *J. Am. Water Resour. Assoc.* **55** 1196–215

Rao E, Ouyang Z, Yu X and Xiao Y 2014 Spatial patterns and impacts of soil conservation service in China *Geomorphology* **207** 64–70

Sahana M, Hong H and Sajjad H 2018 Analyzing urban spatial patterns and trend of urban growth using urban sprawl matrix: A study on Kolkata urban agglomeration, India *Sci. Total Environ.* **628-629** 1557–66

Shadeed S and Almasri M 2010 Application of GIS-based SCS-CN method in West Bank catchments, Palestine *Water Sci. Eng.* **3** 1–13

Shukla S and Gedam S 2018 Evaluating hydrological responses to urbanization in a tropical river basin: A water resources management perspective *Nat. Resour. Res.* **28** 327–47

Trinh D H and Chui T F M 2013 Assessing the hydrologic restoration of an urbanized area via an integrated distributed hydrological model *Hydrol. Earth Syst. Sci.* **17** 4789-801

Verburg P H, Soepboer W, Veldkamp A, Limpiada R, Espaldon V and Mastura S S A 2002 Modeling the spatial dynamics of regional land use: the CLUE-S model *Environ. Manage.* **30** 391–405

Verburg P H, de Koning G H G, Kok K, Veldkamp A and Bouma J 1999 A spatial explicit allocation procedure for modelling the pattern of land use change based upon actual land use *Ecol. Modell.* **116** 45–61

Wang L, Wang H and Wei B 2020 Simulation research on rainfall control effect of low impact development in small town (In Chinese) *South-to-North Water Transfer Water Sci. Technol.* **18** 99–106

Wang Y, Xie X, Liang S L, Zhu B, Yao Y, Meng S and Lu C 2020 Quantifying the response of potential flooding risk to urban growth in Beijing *Sci. Total Environ.* **705** 135863

Wei H, Li R and Yang Q 2002 Research advances of vegetation effect on soil and water conservation in China (In Chinese) *Acta Phytoecologica Sin.* **26** 489–96

Wiering M, Kaufmann M, Mees H, Schellenberger T, Ganzevoort W, Hegger D L T, Larrue C and Matczak P 2017 Varieties of flood risk governance in Europe: how do countries respond to driving forces and what explains institutional change? *Glob. Environ. Change* **44** 15–26

Wing O E, Bates P D, Smith A M, Sampson C C, Johnson K A, Fargione J and Morefield P 2018 Estimates of present and future flood risk in the conterminous United States *Environ. Res. Lett.* **13** 034023

Xu W *et al* 2009 Conservation of giant panda habitat in South Minshan, China, after the May 2008 earthquake *Frontiers in Ecology and the Environment* **7** 353–8

Yang X, Zhou Z, Li J, Fu X, Mu X and Li T 2016 Trade-offs between carbon sequestration, soil retention and water yield in the Guanzhong-Tianshui economic region of China *J. Geog. Sci.* **26** 1449–62

Zhang H, Pang Q, Hua Y, Li X and Liu K 2020 Linking ecological red lines and public perceptions of ecosystem services to manage the ecological environment: A case study in the Fenghen River watershed of Xi'an *Ecol. Indic.* **113** 106218

Zhang K and Chui T F M 2019 Linking hydrological and bioecological benefits of green infrastructures across spatial scales – A literature review *Sci. Total Environ.* **646** 1219–31

Zhao T, Ouyang Z, Wang X, Miao H and Wei Y 2003 Ecosystem services and their valuation of terrestrial surface water system in China (In Chinese) *J. Nat. Res.* **18** 443–52

Zolch T, Henze L, Keilholz P and Pauleit S 2017 Regulating urban surface runoff through nature-based solutions – an assessment at the micro-scale *Environ. Res.* **157** 135–44